Formation and Transformation of $Cu_{2-x}Se_{1-y}Te_y$ Nanoparticles Synthesized by Tellurium Anion Exchange of Copper Selenide

Katherine L. Thompson,[1] Rowan R. Katzbaer,[1] Mauricio Terrones,[1,2,3,5,*] and Raymond E. Schaak[1,4,6,*]

[1] *Department of Chemistry*, [2] *Department of Physics,* [3] *Department of Materials Science and Engineering,* [4] *Department of Chemical Engineering,* [5] *Center for 2-Dimensional and Layered Materials*, *and* [6] *Materials Research Institute, The Pennsylvania State University, University Park, PA 16802, USA*

* Email: res20@psu.edu, mut11@psu.edu

ABSTRACT

Ion exchange reactions of colloidal nanoparticles postsynthetically modify composition while maintaining morphology and crystal structure and therefore are important for tuning properties and producing otherwise inaccessible and/or metastable materials. Reactions involving anion exchange of metal chalcogenides are particularly interesting, as they involve the replacement of the sublattice that defines the structure while also requiring high temperatures that can be disruptive. Here, we show that tellurium anion exchange of weissite $Cu_{2-x}Se$ nanoparticles using a trioctylphosphine-tellurium complex (TOP=Te) yields weissite $Cu_{2-x}Se_{1-y}Te_y$ solid solutions, rather than complete exchange to weissite $Cu_{2-x}Te$, with compositions that are tunable based on the amount of TOP=Te used. Upon storage at room temperature in either solvent or in air, tellurium-rich $Cu_{2-x}Se_{1-y}Te_y$ solid solution nanoparticles transform, over the span of several days, to a selenium-rich $Cu_{2-x}Se_{1-y}Te_y$ composition. The tellurium that is expelled from the solid solution during this process migrates to the surface and forms a tellurium oxide shell, which correlates with the onset of particle agglomeration due to the change in surface chemistry. Collectively, this study demonstrates tunable composition during tellurium anion exchange of copper selenide nanoparticles along with unusual post-exchange reactivity that transforms composition, surface chemistry, and colloidal dispersibility due to the apparent metastable nature of the solid solution product.

INTRODUCTION

The compositions of many types of inorganic nanoparticles can be modified through exchange reactions, which replace cations or anions in a nanoparticle with different cations or anions from solution. This is important, as composition directly impacts properties, which define applications. Such ion exchange reactions generally retain key aspects of morphology and crystal structure, providing a powerful post-synthetic strategy for designing complex nanoparticles with otherwise inaccessible features.[1-11] Copper chalcogenide nanoparticles that have high vacancy concentrations, which are well known plasmonic materials that have different optical properties depending on their compositions,[12] are particularly versatile targets for ion exchange reactions.[13] For example, copper sulfide, copper selenide, and copper telluride nanoparticles can all undergo cation exchange reactions to form derivative metal chalcogenides.[14-20] It is possible to carry out anion exchange reactions on some of these systems as well, but metal chalcogenide anion exchange reactions have been studied much less than cation exchange reactions. The anion sublattice is typically considered to be more rigid than the cation sublattice and the anions have much slower diffusion rates than the cations. These factors necessitate higher temperatures for anion exchange to occur relative to cation exchange.[1,2] The higher temperatures can sometimes be disruptive, interfering with crystal structure and morphology retention and causing Kirkendall voids in the nanoparticles due to imbalances in the diffusion rates of the incoming and outgoing anions during exchange.[1,2,21]

The most common anion exchange reactions of metal chalcogenide nanoparticles transform oxides to sulfides or selenides, sulfides or selenides to tellurides, or convert among semiconductor quantum dot materials, such as cadmium sulfide, cadmium selenide, and cadmium telluride.[22-29] Despite their prevalence in cation exchange, copper chalcogenide nanoparticle anion exchange reactions remain rare. One notable example is the transformation of copper sulfide $Cu_{2-x}S$ into copper telluride $Cu_{2-x}Te$, *via* a series of $Cu_{1-x}S/Cu_{2-x}Te$ intermediates, upon reaction with a complex of trioctylphosphine (TOP) and tellurium, TOP=Te.[27,28] The driving force for this TOP-mediated sulfide-to-telluride anion exchange is the preferential formation of the stronger P=S bond in TOP=S at the expense of the weaker P=Te bond in TOP=Te. A similar driving force would be expected to be applicable to selenide-to-telluride anion exchanges, as the P=Se bond in TOP=Se is also stronger than the P=Te bond in TOP=Te.[29,30]

Here, we describe the tellurium anion exchange of weissite $Cu_{2-x}Se$ using TOP=Te. Rather than forming weissite $Cu_{2-x}Te$ as expected, the selenide-telluride solid solution $Cu_{2-x}Se_{1-y}Te_y$ formed instead. This system, which represents a strategic and rare selenide-to-telluride transformation, provides an instructive example of crystal structure and morphology retention during anion exchange. It also provides useful insights into reaction chemistry, composition control, metastability, surface chemistry, and particle reactivity, which are important characteristics for the applications of colloidal nanoparticles. It also details time-dependent evolution of composition and surface chemistry that can occur during and after anion exchange, which is, to our knowledge, a

type of post-synthetic reactivity that has not been observed in ion-exchanged nanoparticle systems.

EXPERIMENTAL SECTION

Chemicals. Copper (II) acetylacetonate (97%), diphenyl diselenide (97%), oleylamine (70% technical grade), and 1-octadecene (90% technical grade) were purchased from Sigma-Aldrich. Tellurium powder (99.8%, –200 mesh) was purchased from Acros Organics. Trioctylphosphine (>85%) was purchased from TCI America. Analytical grade isopropanol, acetone, hexanes, and ethanol were purchased from VWR. All chemicals were used as received without further purification.

Synthesis of weissite $Cu_{2-x}Se$. Weissite $Cu_{2-x}Se$ nanoparticles were synthesized by a modified literature procedure.[31] Briefly, 130.9 mg $Cu(acac)_2$, 80 mg diphenyl diselenide, and 20 mL oleylamine were combined in a 50 mL three neck flask. The flask was placed under vacuum at 70 ºC for 30 minutes, and then the temperature was raised to 140 ºC for an additional 30 minutes before being placed under an Ar atmosphere. The flask was then heated to 220 ºC at a rate of approx. 6 ºC/min, after which a 3-minute timer was started as the flask reached 215 ºC. After 3 minutes, the flask was rapidly cooled in a water bath to bring it to room temperature. The particles were washed in a 1:1 mixture of acetone and IPA two times, collected by centrifugation at 14000 rpm for 3 minutes, and stored in hexanes for future characterization.

Te anion exchange. Tellurium exchange was carried out using a minor modification of a literature procedure.[27] Briefly, 5 mL octadecene and Te powder (amounts given below) were combined in a 25 mL three neck flask and placed under vacuum at 120 ºC, for 30 minutes. The amount of Te varied depending on the targeted extent of exchange and was in the range of 3.1 mg for a ¼ exchange to 31.0 mg for a 5-times excess exchange. The flask was then placed under an Ar atmosphere before 2 mL of TOP was injected. The flask was then heated to 260 ºC at a rate of approx. 9 ºC/min and held for 30 minutes to create the yellow TOP=Te complex. While the flask was at 260 ºC, 10-20 mg of the weissite $Cu_{2-x}Se$ nanoparticles were vacuum dried in a 20 mL vial and resuspended in oleylamine. For lesser extents of anion exchange, 20 mg of $Cu_{2-x}Se$ particles were used such that the mass of Te powder required would be a more reasonable quantity to mass. The suspended particles were placed under vacuum for 30 minutes before being put under an Ar atmosphere, and then the suspended particles were sonicated for 10 minutes. Finally, the particles were rapidly injected into the flask at 260 ºC and left to react for 15 minutes. After the reaction, the flask was lifted off the heat to cool to 210 ºC before being quenched in a room temperature water bath. The exchanged particles were then washed once with ethanol and once with a 4:1 mixture of ethanol and hexanes and collected by centrifugation at 14000 rpm for 3 minutes. The particles were then resuspended in hexanes and stored for future characterization. To study thermal stability, a sample was drop cast on a silicon wafer and sealed in a quartz tube that had been evacuated to a pressure of 10^{-4} torr. The tube was then placed in a Carbolite 1300 box furnace. The furnace was heated to 400 ºC over 30 minutes and held at this temperature for 1 hour. The furnace was then allowed to cool ambiently to room temperature.

Characterization. All transmission electron microscopy (TEM) images were collected using an FEI Tecnai G20 20 XTWIN microscope operating at 200 kV. High-angle annular dark-field scanning transmission electron microscopy (HAADF-STEM) images, and STEM energy-dispersive X-ray spectroscopy (STEM-EDS) elemental maps were collected on an FEI Talos F200X S/TEM at an accelerating voltage of 200 kV. TEM images were analyzed using ImageJ software. Bruker ESPRIT 2 software was used to analyze and generate STEM-EDS elemental map data, where the Cu Kα, Se Kα, and Te Lα EDS lines were mapped. An Empyrean diffractometer using Cu Kα radiation was used to collect powder X-ray diffraction (XRD) data for all materials. CrystalMaker and CrystalDiffract from CrystalMaker Software Ltd., Oxford, England, were used to simulate crystal structure and powder diffraction patterns. The simulated XRD patterns corresponding to the anion solid solution samples (Table S1) were obtained by modifying the lattice parameters and site occupancies according to Vegard's law, as described in the Supporting Information. Samples for X-ray photoelectron spectroscopy (XPS) were prepared by allowing the suspended material to dry in a small, plastic tube, so as to avoid the possible contamination of leaching from a glass container. The base of the tube was flattened by cutting and then the bottom of the tube containing the sample was removed. This created a flat plastic dish filled with an even amount of sample. XPS spectra were collected using a Physical Electronics VersaProbe II instrument equipped with a monochromatic Al Kα X-ray source ($h\nu$ = 1,486.7 eV) and a concentric hemispherical analyzer. Charge neutralization was performed using both low energy electrons (<5 eV) and argon ions. The binding energy axis was calibrated using sputter cleaned Cu (Cu $2p_{3/2}$ = 932.62 eV, Cu $3p_{3/2}$ = 75.1 eV) and Au (Au $4f_{7/2}$ = 83.96 eV) foils. Peaks were charge referenced to the CH_x band in the carbon 1s spectra at 285 eV. Measurements were made at a takeoff angle of 45º with respect to the sample surface plane. This resulted in a typical sampling depth of 3-6 nm (95% of the signal originated from this depth or shallower).

RESULTS AND DISCUSSION

Colloidal nanoparticles of weissite $Cu_{2-x}Se$ were synthesized by heating a mixture of $Cu(acac)_2$, diphenyl diselenide, and oleylamine at 215 ºC for 3 min under an Ar atmosphere;[30] complete details are provided in the Experimental Section. Exchange of the selenium in the $Cu_{2-x}Se$ nanoparticles with tellurium was attempted by reacting them with a stoichiometric amount of TOP=Te in oleylamine at 260 ºC, which was the temperature previously found to be optimal for tellurium anion exchange in metal chalcogenide nanoparticles,[27] for 15 minutes. Figure 1a shows a TEM image of the $Cu_{2-x}Se$ nanoparticles, which appear as hexagonal plates. In the TEM image, some of the $Cu_{2-x}Se$ plates are oriented parallel to the substrate (*i.e.*, those that appear as larger hexagons) while the majority (*i.e.*, those that appear as smaller elongated hexagons) are stacked side-to-side. The $Cu_{2-x}Se$ plates oriented side-to-side have an average thickness of 10 ± 2 nm and an average length of 14 ± 2 nm; the length of the side-oriented plates corresponds to the point-to-point length of the top-down oriented plates. Figure 1b shows a TEM image of the tellurium-exchanged product, which looks morphologically similar to the $Cu_{2-x}Se$ precursor and has an average thickness and length of 10 ± 2 nm and 16 ± 2

nm, respectively. Morphology and size are therefore retained, which is generally diagnostic of anion exchange reactions. A competing dissolution and reprecipitation pathway was ruled out, as a copper telluride product did not form under comparable conditions without $Cu_{2-x}Se$ being present. Additionally, dissolution of $Cu_{2-x}Se$ required heating to 300 ºC, and precipitation of solid products after dissolution only occurred upon cooling.

Powder XRD patterns for the $Cu_{2-x}Se$ precursor and the product formed after reaction with TOP=Te are shown in Figure 1c. The XRD pattern for the copper selenide particles matches well with that of a simulated pattern for weissite $Cu_{2-x}Se$ that incorporates small amounts of preferred orientation, as well as site occupancy optimization, as discussed in the Supporting Information (Figure S1). The XRD pattern for the tellurium-exchanged product matches qualitatively with that of weissite $Cu_{2-x}Te$ (Figure S2), but the peaks are shifted to higher two theta values, which correlates with smaller lattice parameters than those expected for $Cu_{2-x}Te$. This observation suggests the possibility that a $Cu_{2-x}Se_{1-y}Te_y$ solid solution formed instead of $Cu_{2-x}Te$ upon tellurium exchange of weissite $Cu_{2-x}Se$.

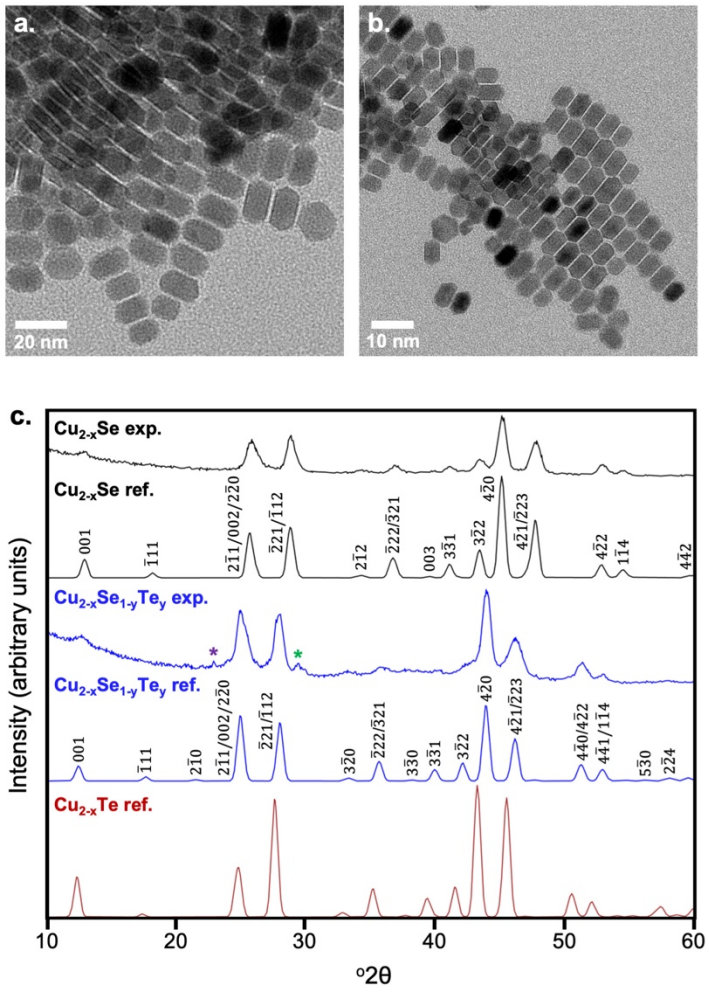

Figure 1. TEM and XRD data for $Cu_{2-x}Se$ nanoparticles and the product of Te anion exchange, which is a $Cu_{2-x}Se_{1-y}Te_y$ Se/Te solid solution. TEM images of a collection of (a) $Cu_{2-x}Se$ nanoparticles before Te anion exchange and (b) $Cu_{2-x}Se_{1-y}Te_y$ solid solution

nanoparticles formed after exchange. (c) Experimental XRD patterns for $Cu_{2-x}Se$ and the $Cu_{2-x}Se_{1-y}Te_y$ solid solution product, along with reference patterns for weissite $Cu_{2-x}Se$,[31] weissite $Cu_{2-x}Te$,[32] and $Cu_{2-x}Se_{1-y}Te_y$ (as discussed in the text) for comparison. The purple asterisk (*) corresponds to a Te impurity and the green asterisk (*) corresponds to a TeO_2 impurity.

The formation of a solid solution is validated by the HAADF-STEM image and corresponding STEM-EDS element maps in Figure 2a, which show co-localization of Se and Te, along with Cu, throughout the particles. The STEM-EDS element maps reveal a Te-rich surface. This observation suggests that the tellurium anion exchange reaction is diffusion limited and therefore unable to fully exchange the Se under the reaction conditions studied. Additionally, this suggests that the selenide-telluride solid solution nanoparticles may become coated with a thin, amorphous tellurium oxide shell over time. Analysis of the STEM-EDS maps in Figure 2a reveals an average composition of $Cu_{2-x}Se_{0.38}Te_{0.62}$ for the particles formed upon tellurium exchange of $Cu_{2-x}Se$; an ensemble EDS spectrum is shown in Figure 2b. Assuming that Vegard's law is applicable to this solid-solution system, we estimated the expected lattice parameter values for $Cu_{2-x}Se_{0.38}Te_{0.62}$. The lattice parameters for weissite $Cu_{2-x}Se$ are a = 8.04 Å and c = 6.84 Å while those for weissite $Cu_{2-x}Te$ are a = 8.37 Å and c = 7.16 Å.[31,32] Using Vegard's law (*i.e.*, a weighted average) for the a and c lattice parameters independently, we estimate that for $Cu_{2-x}Se_{0.38}Te_{0.62}$, a = 8.24 Å and c = 7.04 Å. These lattice parameters, along with random mixing of 38% Se and 62% Te on all chalcogen sites and incorporation of a similar preferred orientation and site occupancy optimization used for $Cu_{2-x}Se$, were used to generate the reference pattern for the tellurium-exchanged product in Figure 1c. The experimental and simulated patterns match well. Additionally, the lattice expansion observed by XRD is qualitatively consistent with the slight expansion in particle length observed by TEM, noting that expected expansion in particle thickness is within the standard deviation of the thickness measurements. Attempts to push the tellurium exchange completely to $Cu_{2-x}Te$, with excess TOP=Te, resulted in the concomitant formation of Te and TeO_2, which also begin to show up as minor impurities in the $Cu_{2-x}Se_{0.38}Te_{0.62}$ sample (Figure S3).

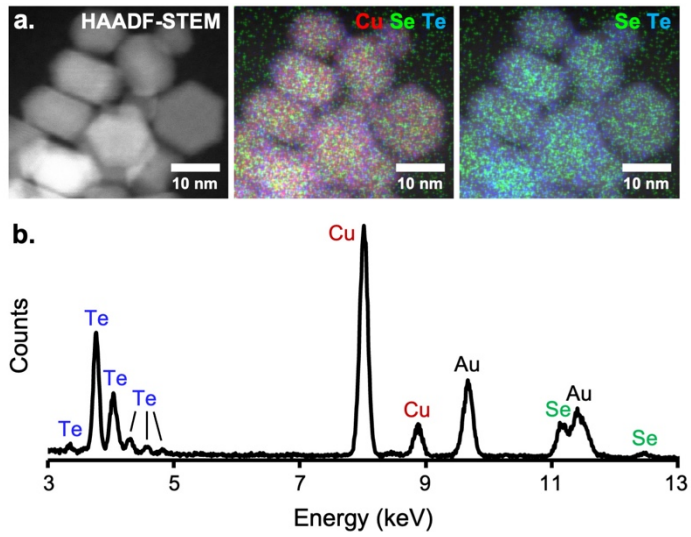

Figure 2. (a) HAADF-STEM image and corresponding STEM-EDS element maps showing overlays of various combinations of Cu (red), Se (green), and Te (blue) for the $Cu_{2-x}Se_{0.38}Te_{0.62}$ solid solution nanoparticles. (b) Ensemble EDS spectrum corresponding to the sample in (a), showing the presence of Cu, Te, and Se. The Au signal comes from the Au TEM grid.

As mentioned above, attempted stoichiometric tellurium exchange of $Cu_{2-x}Se$ led to the formation of the tellurium-rich $Cu_{2-x}Se_{0.38}Te_{0.62}$ solid solution and attempts to incorporate more tellurium using excess TOP=Te resulted in an increase in tellurium-based impurities, including Te and TeO_2. We therefore studied substoichiometric tellurium exchange reactions on $Cu_{2-x}Se$ to understand the extent of solid solution tunability that can be achieved. Figure 3a shows powder XRD data for various substoichiometric exchange reactions, as well as $Cu_{2-x}Se$ and the stoichiometric and excess exchange products (which both have Te-rich impurities relative to the lesser Te exchanges, as discussed) for comparison; an enlargement of the peaks between 40 and 50 º2θ is provided in Figure 3b. (All lattice parameters determined using Vegard's law for the XRD patterns in Figure 3 are included in Table S2.)

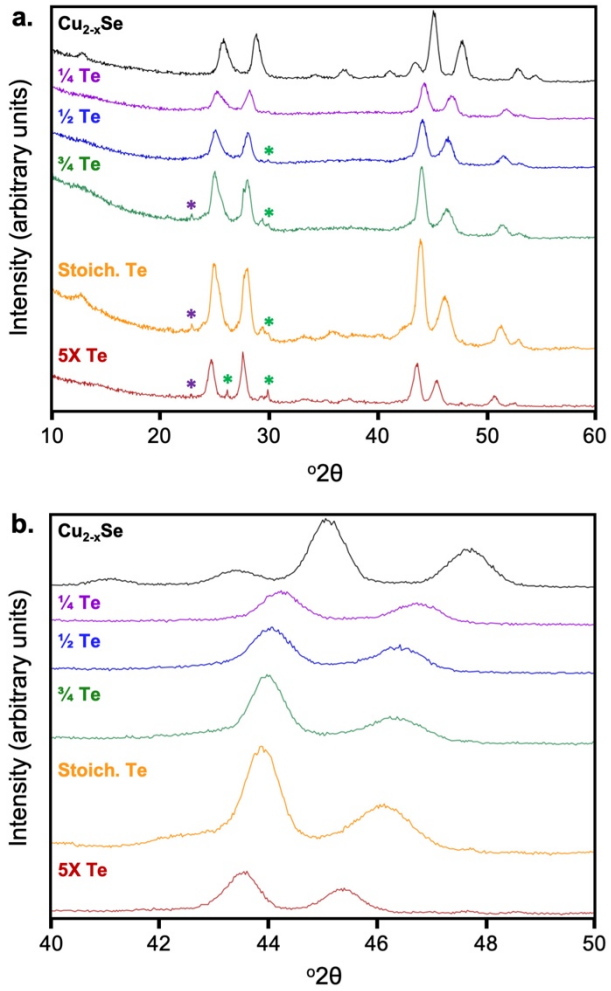

Figure 3. XRD patterns for (a) the products of various substoichiometric, stoichiometric, and excess Te anion exchange reactions applied to $Cu_{2-x}Se$ and (b) an enlargement of the region from 40 to 50 º2θ, showing that the peaks shift to the left as more Te is incorporated. The purple asterisk (*) corresponds to a Te impurity and the green asterisk (*) corresponds to a TeO_2 impurity.

A progressive shift of peak positions is observed, suggesting the formation of composition-tunable solid solutions with increasing lattice constants as the Te content increases. Interestingly, the weaker reflections that are characteristic of the weissite phases are mostly suppressed in the intermediate exchanges. This could possibly be due to the formation of the higher-symmetry wurtzite variant of $Cu_{2-x}Se$, which would be expected to retain the most-intense peaks but not have the lower-intensity peaks.[33,34] However, given the observation that the precursor and Te-rich product both adopt the weissite structure, it is more likely that the intermediate members are weissite as well. We speculate that these intermediate solid solutions have lower crystallinity, which structurally would blur the distinction between weissite and wurtzite. This possibility is consistent with the XRD patterns in Figure 3b, which show non-zero background in the region where the weissite $(3\bar{2}0), (2\bar{2}2), (003), (3\bar{3}1)$, and $(3\bar{2}2)$ reflections would be

expected. This observation suggests that these low-intensity peaks are just broadened to the point where they are not discernable as distinct peaks but rather contribute to a broader above-baseline hump in the same region.

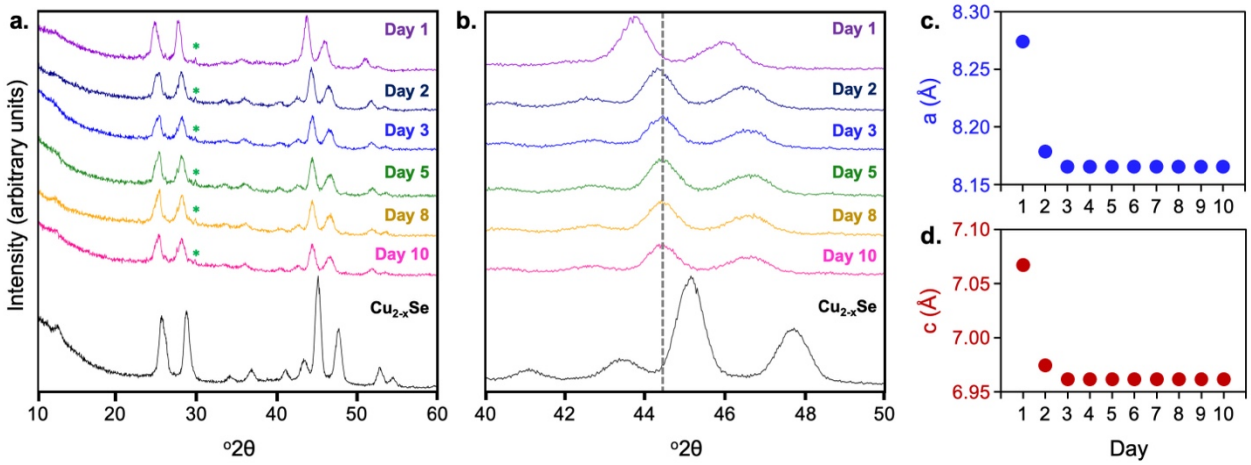

Figure 4. (a) XRD patterns and (b) an enlargement of the region from 40 to 50 º2θ for a sample of $Cu_{2-x}Se_{1-y}Te_y$ stored in hexanes over the course of 10 days. The green asterisk (*) corresponds to a TeO_2 impurity and $Cu_{2-x}Se$ is shown for comparison. (c) and (d) show plots of the *a* and *c* lattice parameters, respectively, for the $Cu_{2-x}Se_{1-y}Te_y$ sample each day of storage.

Weissite $Cu_{2-x}Se$ nanoparticles have been shown to be metastable, transforming to the more stable berzelianite phase upon heating,[31] while weissite $Cu_{2-x}Te$ is a stable phase.[32] We were therefore interested in probing the stability of the $Cu_{2-x}Se_{1-y}Te_y$ solid solution. Nanoparticles of $Cu_{2-x}Se_{1-y}Te_y$ were therefore drop cast onto a silicon wafer, vacuum sealed in a quartz tube, and heated to 400 ºC for 1 hour. Under these conditions, the particles transformed to a phase matching that of β-$Cu_{2-x}Se$,[35] but with expanded lattice indicating that indicates the selenide-telluride solid solution remains (Figure S4). This result is also consistent with $Cu_{2-x}Se_{1-y}Te_y$ being metastable. Interestingly, this result highlights differences in phase stability and accessibility for selenide versus selenide-telluride composition. Specifically, it indicates that berzelianite, which is the stable phase for $Cu_{2-x}Se$, is not the phase that $Cu_{2-x}Se_{1-y}Te_y$ transforms to upon heating.

In addition to thermal stability, we were interested in probing the stability over time. The particles are dispersed in hexanes for storage, so we began by extracting aliquots from a stored stoichiometric exchange sample every day for 10 days and characterizing the isolated powder product by XRD, shown in Figure 4a; an enlargement of the peaks between 40 and 50 º2θ is provided in Figure 4b. The starting nanoparticles (labeled as "Day 1") had an average composition of $Cu_{2-x}Se_{0.29}Te_{0.71}$, based on Vegard's law and the observed lattice parameters of *a* = 8.274 Å and *c* = 7.067 Å. After only one day of storage in hexanes (labeled as "Day 2"), the XRD pattern for the isolated nanoparticles had shifted significantly, with the lattice parameters decreasing to *a* = 8.179 Å and *c* = 6.974 Å, which corresponds (*via* Vegard's law) to a Se-rich composition of $Cu_{2-x}Se_{0.58}Te_{0.42}$. On "Day 3", the lattice parameters further decreased to a = 8.165 Å and c = 6.962 Å, which

corresponds to a composition of $Cu_{2-x}Se_{0.62}Te_{0.38}$. No further change in lattice parameters was observed beyond this point, suggesting equilibration to $Cu_{2-x}Se_{0.62}Te_{0.38}$, which has an approximate 2:3 ratio of Te:Se. Note that to obtain the data in Figure 4a and 4b, we studied a Te-rich sample with a small crystalline TeO_2 impurity that could serve as an internal standard, for purposes of both validating the solid solution peak shifts and confirming that any changes in composition of the solid solution do not impact other components of the sample, *i.e.*, through transferring Te from the solid solution nanoparticles to the TeO_2 impurity. Indeed, the TeO_2 peak positions and relative intensities do not shift, despite shifts in the solid solution peaks. Figure 4c and 4d compile the lattice parameter and composition data for all 10 days, showing the rapid change followed by leveling off. Similar time dependent XRD data were acquired for dried nanoparticle samples stored as a powder, rather than as a colloidal dispersion in hexanes, shown in Figure 5a; an enlargement of the peaks between 40 and 50 º2θ is provided in Figure 5b. This dried sample exhibited similar behavior to that of the sample stored in hexanes, as the greatest shift in lattice parameters was observed between days 1 and 2, with a slight shift between days 2 and 3 and leveling off beyond that.

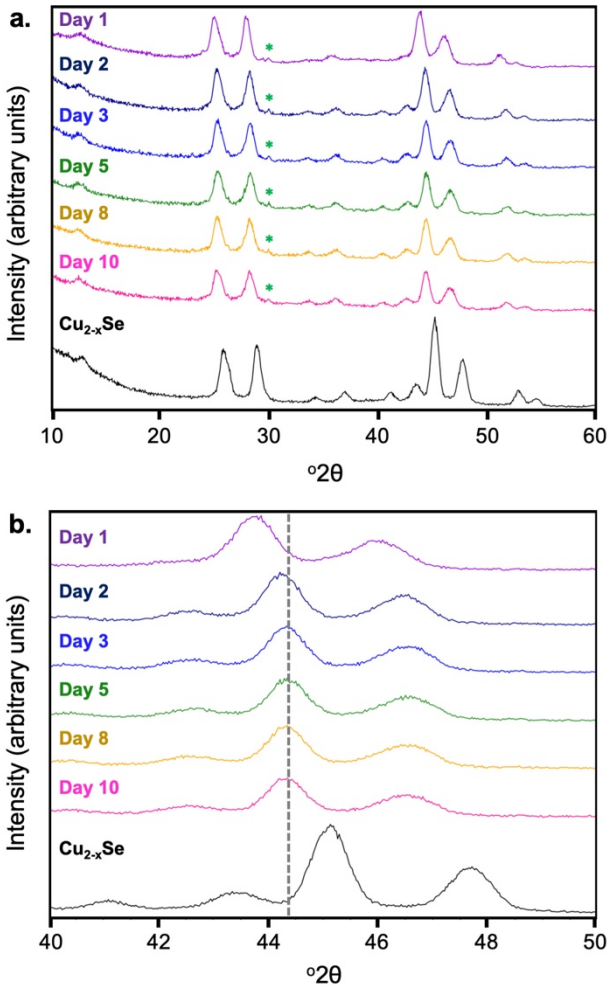

Figure 5. (a) XRD patterns and (b) an enlargement of the region from 40 to 50 º2θ for a sample of $Cu_{2-x}Se_{1-y}Te_y$ stored in air over the course of 10 days. The green asterisk (*) corresponds to a TeO_2 impurity and $Cu_{2-x}Se$ is shown for comparison.

The time-dependent XRD data in Figure 4 indicate that the most Te-rich $Cu_{2-x}Se_{1-y}Te_y$ solid solution nanoparticles are not stable and decompose to Se-rich $Cu_{2-x}Se_{0.62}Te_{0.38}$, which appears to be stable on the timescale interrogated. This observation indicates both that the Te anion exchange reaction generates a metastable product and that the metastable product changes composition over time, which is important for understanding the reactivity, stability, and applicability of colloidal nanoparticles synthesized through such post-synthetic modification processes. Interestingly, despite the shifts in lattice parameters that correlate to a change in solid solution composition, EDS quantifications show nearly identical Se:Te ratios across the entire 10-day window that the particles were interrogated. To rationalize this behavior, we used XPS to study the tellurium on the surface, noting that the STEM-EDS data in Figure 2a indicated a Te-rich surface.

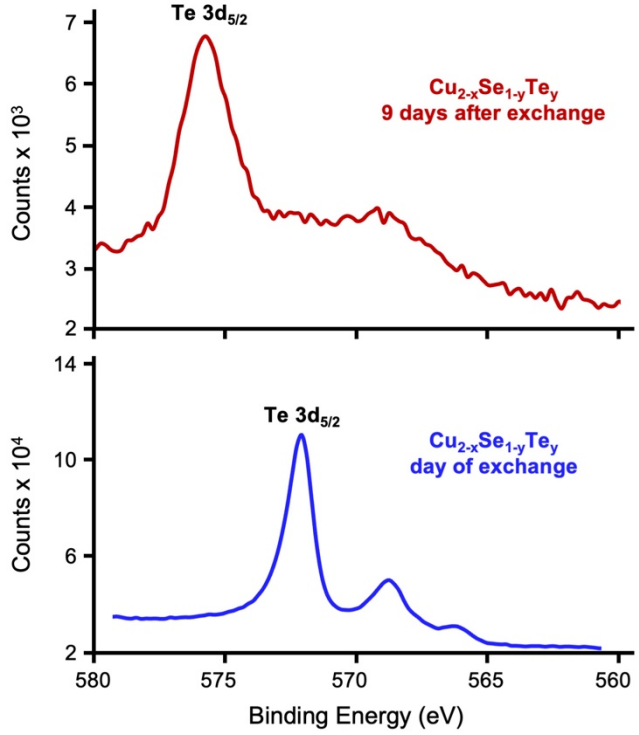

Figure 6. XPS data for $Cu_{2-x}Se_{1-y}Te_y$ acquired on the same day as anion exchange and after being stored in hexanes and exposed to air for 9 days, showing the shift in the Te $3d_{5/2}$ peak from a binding energy consistent with Te^{2-} (*i.e.*, $Cu_{2-x}Se_{1-y}Te_y$) to one that is consistent with Te^{4+} (*i.e.*, TeO_2).

Figure 6 shows high resolution XPS spectra of the Te $3d_{5/2}$ region for a tellurium-exchanged sample analyzed the same day of the reaction and a sample that had been stored in air. For the sample analyzed on the same day it was synthesized, the primary

Te $3d_{5/2}$ peak was at 572.2 eV, which is consistent with Te^{2-}, the oxidation state expected for $Cu_{2-x}Se_{1-y}Te_y$;[36] there was no evidence of oxidized tellurium in this sample. (The sample in Figure 2a, which showed a Te-rich shell by STEM-EDS, had not been analyzed as rapidly after synthesis as the sample analyzed by XPS, which showed no Te enrichment or oxidation.) The peak at 568.6 eV corresponds to the Cu LMM Auger peak.[37] However, for the sample analyzed after storage in air, the primary Te $3d_{5/2}$ peak shifted to 575.8 eV, which is consistent with that of Te^{4+} in TeO_2 and therefore indicates surface oxidation.[38]

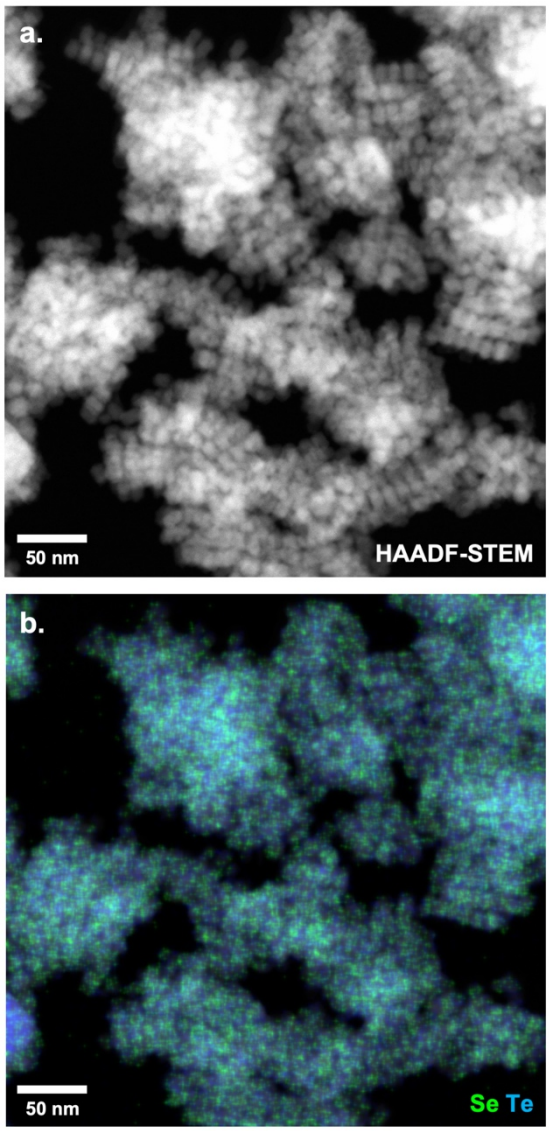

Figure 7. (a) HAADF-STEM image and (b) corresponding STEM-EDS element maps for Se and Te (overlaid) of agglomerated $Cu_{2-x}Se_{1-y}Te_y$ nanoparticles after storage in hexanes and exposure to air.

The XPS results therefore support the formation of a TeO_2 shell around the tellurium-exchanged particles over time as the sample is stored. There are two important consequences of this observation. First, this progressive development of a TeO_2 surface helps to rationalize the time-dependent composition change of the crystalline component of the tellurium-exchanged nanoparticles. XRD showed a shift from a Te-rich to a Se-rich $Cu_{2-x}Se_{1-y}Te_y$ solid solution while the overall composition by EDS did not change. This behavior, coupled with the XPS data, suggests that some of the tellurium is expelled from the Te-rich solid solution to form Se-rich $Cu_{2-x}Se_{0.62}Te_{0.38}$, and the expelled tellurium oxidizes and forms a shell around the nanoparticles rather than being dissolved into solution or forming separate particles. The XRD peaks for the crystalline TeO_2 impurity present from the beginning, highlighted in the XRD patterns in Figure 5a, do not change in position or relative intensity throughout this time-dependent progression, suggesting that the tellurium oxide shell that develops is amorphous, as it does not increase the apparent amount of crystalline TeO_2 observed by XRD. Second, the TEM and HAADF-STEM images, along with the STEM-EDS element maps, in Figures 1 and 2 show well dispersed and discreet $Cu_{2-x}Se_{0.38}Te_{0.62}$ particles, while those in Figure 7 show agglomerated particles after storage. The particles that have developed a significant tellurium oxide shell, *i.e.*, those that were found by XRD to have transformed their composition to the Se-rich $Cu_{2-x}Se_{0.62}Te_{0.38}$ and by XPS to have a TeO_2 surface, are agglomerated and no longer discreet. We surmise that the native ligands that cap the surface of the $Cu_{2-x}Se_{1-y}Te_y$ solid solution nanoparticles do not bind as well to tellurium oxide, and therefore compromise colloidal dispersibility in favor of agglomeration. This result, which further characterizes the time-dependent transformations in the $Cu_{2-x}Se_{1-y}Te_y$ solid solution nanoparticles, indicates that storage (*i.e.*, the amount of time post-synthesis) impacts composition, reactivity, surface chemistry, and colloidal stability. Ligand exchange, or multi-ligand surfaces, may be worth exploring in the future to help mitigate such transformations.

CONCLUSIONS

Here, we demonstrated that tellurium anion exchange of weissite $Cu_{2-x}Se$ nanoparticles produces $Cu_{2-x}Se_{1-y}Te_y$ solid solutions with tunable compositions, rather than fully exchanged $Cu_{2-x}Te$. This contrasts prior work with tellurium anion exchange of copper sulfide, which produced a heterostructured telluride/sulfide product rather than a solid solution[27] and points to different classes of products, *i.e.*, solid solutions *vs*. heterostructured, that can be accessible *via* nanoparticle anion exchange. Most notably, we discovered unusual reactivity that transforms composition, surface chemistry, and colloidal dispersibility over time when the tellurium-exchanged nanoparticles are stored in either solvent or in air, while maintaining morphology and structure. This is useful knowledge when one considers the applications of nanoparticles, where compositional and colloidal stability are important. These results showcase how key features of nanoparticles can evolve and how their evolution can be understood and rationalized. Overall, this study adds important new knowledge about anion exchange reactions of metal chalcogenide nanoparticles, which are much less studied than cation exchange reactions and have been limited to only a few systems.

ASSOCIATED CONTENT

SUPPORTING INFORMATION

Additional XRD data with detailed descriptions of modified reference patterns and crystallographic information for the different solid solutions. This material is available free of charge via the Internet at http://pubs.acs.org.

AUTHOR INFORMATION

Corresponding Authors

Raymond E. Schaak – *Department of Chemistry*, *Department of Chemical Engineering*, and *Materials Research Institute*, *The Pennsylvania State University, University Park, Pennsylvania 16802, United States*; Email: res20@psu.edu

Mauricio Terrones –*Department of Chemistry*, *Department of Physics, Department of Materials Science and Engineering, and Center for 2-Dimensional and Layered Materials*, *The Pennsylvania State University, University Park, PA 16802, United States;* Email: mut11@psu.edu

Authors

Katherine L. Thompson – *Department of Chemistry*, *The Pennsylvania State University, University Park, Pennsylvania 16802, United States*

Rowan R. Katzbaer – *Department of Chemistry*, *The Pennsylvania State University, University Park, Pennsylvania 16802, United States*

Notes

The authors declare no competing financial interest.

ACKNOWLEDGMENT

This work was supported by the U.S. National Science Foundation under grant DMR-2210442. TEM, XRD, and XPS data were acquired at the Materials Characterization Lab of the Penn State Materials Research Institute. The authors thank Prof. Katherine Plass and Gaurav Dey for helpful discussions.

REFERENCES

(1) Saruyama, M.; Sato, R.; Teranishi, T. Transformations of Ionic Nanocrystals via Full and Partial Ion Exchange Reactions. *Acc. Chem. Res.* **2021**, *54* (4), 765–775.

(2) Anderson, B. D.; Tracy, J. B. Nanoparticle Conversion Chemistry: Kirkendall Effect, Galvanic Exchange, and Anion Exchange. *Nanoscale* **2014**, *6* (21), 12195–12216.

(3) De Trizio, L.; Manna, L. Forging Colloidal Nanostructures via Cation Exchange Reactions. *Chem. Rev.* **2016**, *116* (18), 10852–10887.

(4) Son, D. H.; Hughes, S. M.; Yin, Y. D.; Alivisatos, A. P. Cation exchange reactions in ionic nanocrystals. *Science.* **2004**, *306*, 1009-1012.

(5) Fenton, J.L.; Steimle, B.C.; Schaak, R.E. Tunable Intraparticle Frameworks for Creating Complex Heterostructured Nanoparticle Libraries. *Science* **2018**, *360*, 513-517.

(6) Steimle, B. C.; Fenton, J. L.; Schaak, R. E. Rational Construction of a Scalable Heterostructured Nanorod Megalibrary. *Science* **2020**, *367* (6476), 418–424.

(7) Li, Z.; Saruyama, M.; Asaka, T.; Tatetsu, Y.; Teranishi, T. Determinants of crystal structure transformation of ionic nanocrystals in cation exchange reactions. *Science* **2021**, *373*, 332-337.

(8) Enright, M. J.; Cossairt, B. M. Synthesis of Tailor-Made Colloidal Semiconductor Heterostructures. *Chem. Commun.* **2018**, *54* (52), 7109–7122.

(9) Rivest, J. B.; Jain, P. K. Cation Exchange on the Nanoscale: An Emerging Technique for New Material Synthesis, Device Fabrication, and Chemical Sensing. *Chem. Soc. Rev.* **2013**, *42* (1), 89–96.

(10) Coughlan, C.; Ibáñez, M.; Dobrozhan, O.; Singh, A.; Cabot, A.; Ryan, K. M. Compound Copper Chalcogenide Nanocrystals. *Chem. Rev.* **2017**, *117* (9), 5865-6109.

(11) Li, H.; Zanella, M.; Genovese, A.; Povia, M.; Falqui, A.; Giannini, C.; Manna, L. Sequential Cation Exchange in Nanocrystals: Preservation of Crystal Phase and Formation of Metastable Phases. *Nano Lett.* **2011**, *11*, 4964-4970.

(12) Kriegel, I.; Jiang, C.; Rodríguez-Fernández, J.; Schaller, R. D.; Talapin, D. V.; da Como, E.; Feldmann, J. Tuning the Excitonic and Plasmonic Properties of Copper Chalcogenide Nanocrystals. *J. Am. Chem. Soc.* **2012**, *134* (3), 1583-1590.

(13) Lesnyak, V.; Brescia, R.; Messina, G. C.; Manna, L. Cu Vacancies Boost Cation Exchange Reactions in Copper Selenide Nanocrystals. *J. Am. Chem. Soc.* **2015**, *137* (29), 9315–9323.

(14) Liu, M.; Liu, Y.; Gu, B.; Wei, X.; Xu, G.; Wang, X.; Swihart, M.T.; Yong, K.-T. Recent advances in copper sulphide-based nanoheterostructures. *Chem. Soc. Rev.* **2019**, *48*, 4950-4965.

(15) Ha, D.-H.; Caldwell, A. H.; Ward, M. J.; Honrao, S.; Mathew, K.; Hovden, R.; Koker, M. K. A.; Muller, D. A.; Hennig, R. G.; Robinson, R. D. Solid–Solid Phase Transformations Induced through Cation Exchange and Strain in 2D Heterostructured Copper Sulfide Nanocrystals. *Nano Lett.* **2014**, *14*, 7090– 7099.

(16) Hernandez-Pagan, E.A.; O'Hara, A.; Arrowood, S.L.; McBride, J.R.; Rhodes, J.M.; Pantelides, S.T.; Macdonald, J.E. Transformation of the Anion Sublattice in the

Cation-Exchange Synthesis of Au_2S from $Cu_{2-x}Se$ Nanocrystals. *Chem. Mater.* **2018**, *30*, 8843-8851.

(17) Gariano, G.; Lesnyak, V.; Brescia, R.; Bertoni, G.; Dang, Z.; Gaspari, R.; De Trizio, L.; Manna, L. Role of the Crystal Structure in Cation Exchange Reactions Involving Colloidal Cu_2Se Nanocrystals. *J. Am. Chem. Soc.* **2017**, *139* (28), 9583–9590.

(18) Tu, R.; Xie, Y.; Bertoni, G.; Lak, A.; Gaspari, R.; Rapallo, A.; Cavalli, A.; De Trizio, L.; Manna, L. Influence of the Ion Coordination Number on Cation Exchange Reactions with Copper Telluride Nanocrystals. *J. Am. Chem. Soc.* **2016**, *138*, 7082-7090.

(19) Li, H.; Brescia, R.; Povia, M.; Prato, M.; Bertoni, G.; Manna, L.; Moreels, I. Synthesis of Uniform Disk-Shaped Copper Telluride Nanocrystals and Cation Exchange to Cadmium Telluride Quantum Disks with Stable Red Emission. *J. Am. Chem. Soc.* **2013**, *135*, 12270-12278.

(20) Kriegel, I.; Rodríguez-Fernández, J.; Wisnet, A.; Zhang, H.; Waurisch, C.; Eychmüller, A.; Dubavik, A.; Govorov, A. O.; Feldmann, J. Shedding Light on Vacancy-Doped Copper Chalcogenides: Shape-Controlled Synthesis, Optical Properties, and Modeling of Copper Telluride Nanocrystals with Near-Infrared Plasmon Resonances. *ACS Nano* **2013**, *7* (5), 4367–4377.

(21) Yang, Z.; Yang, N.; Pileni, M.-P. Nano Kirkendall Effect Related to Nanocrystallinity of Metal Nanocrystals: Influence of the Outward and Inward Atomic Diffusion on the Final Nanoparticle Structure. *J. Phys. Chem. C* **2015**, *119* (39), 22249–22260.

(22) Lim, Y.; Lee, C.-H.; Jun, C.-H.; Kim, K.; Cheon, J. Morphology-Conserving Non-Kirkendall Anion Exchange of Metal Oxide Nanocrystals. *J. Am. Chem. Soc.* **2020**, *142* (20), 9130–9134.

(23) Park, J.; Zheng, H.; Jun, Y.-W.; Alivisatos, A.P. Hetero-Epitaxial Anion Exchange Yields Single-Crystalline Hollow Nanoparticles. *J. Am. Chem. Soc.* **2009**, *131*, 13943-13945.

(24) Dawood, F.; Schaak, R. E. ZnO-Templated Synthesis of Wurtzite-Type ZnS and ZnSe Nanoparticles. *J. Am. Chem. Soc.* **2009**, *131* (2), 424–425.

(25) Hodges, J. M.; Kletetschka, K.; Fenton, J. L.; Read, C. G.; Schaak, R. E. Sequential Anion and Cation Exchange Reactions for Complete Material Transformations of Nanoparticles with Morphological Retention. *Angew. Chem.* **2015**, *127* (30), 8793–8796.

(26) Sines, I. T.; Vaughn, D. D.; Biacchi, A. J.; Kingsley, C. E.; Popczun, E. J.; Schaak, R. E. Engineering Porosity into Single-Crystal Colloidal Nanosheets Using Epitaxial Nucleation and Chalcogenide Anion Exchange Reactions: The Conversion of SnSe to SnTe. *Chem. Mater.* **2012**, *24* (15), 3088–3093.

(27) Garcia-Herrera, L. F.; McAllister, H. P.; Xiong, H.; Wang, H.; Lord, R. W.; O'Boyle, S. K.; Imamovic, A.; Steimle, B. C.; Schaak, R. E.; Plass, K. E. Multistep

Regioselectivity and Non-Kirkendall Anion Exchange of Copper Chalcogenide Nanorods. *Chem. Mater.* **2021**, *33* (10), 3841–3850.

(28) Espinosa, A. R.; Novak, M.; Luo, Q.; Hole, B.; Doligon, C.; Prenza Sosa, K.; Gray, J. L.; Rossi, D. P.; Plass, K. E. Heterostructures of $Cu_{2-x}S/Cu_{2-x}Te$ Plasmonic Semiconductors: Disappearing and Reappearing LSPR with Anion Exchange. *Chem. Commun*. **2022**, *58* (70), 9810–9813.

(29) Saruyama, M.; So, Y.-G.; Kimoto, K.; Taguchi, S.; Kanemitsu, Y.; Teranishi, T. Spontaneous Formation of Wurzite-CdS/Zinc Blende-CdTe Heterodimers through a Partial Anion Exchange Reaction. *J. Am. Chem. Soc.* **2011**, *133* (44), 17598–17601.

(30) Sines, I. T.; Schaak, R. E. Phase-Selective Chemical Extraction of Selenium and Sulfur from Nanoscale Metal Chalcogenides: A General Strategy for Synthesis, Purification, and Phase Targeting. *J. Am. Chem. Soc.* **2011**, *133* (5), 1294–1297.

(31) Lord, R. W.; Fanghanel, J.; Holder, C. F.; Dabo, I.; Schaak, R. E. Colloidal Nanoparticles of a Metastable Copper Selenide Phase with Near-Infrared Plasmon Resonance. *Chem. Mater.* **2020**, *32* (23), 10227–10234.

(32) Yu, L.; Luo, K.; Chen, S.; Duan, C.-G. Cu-Deficiency Induced Structural Transition of $Cu_{2-x}Te$. *CrystEngComm* **2015**, *17* (14), 2878–2885.

(33) Hernandez-Pagan, E.A.; Robinson, E.H.; La Croix, A.D.; Macdonald, J.E. Direct Synthesis of Novel $Cu_{2-x}Se$ Wurtzite Phase. *Chem. Mater.* **2019**, *31*, 4619-4624.

(34) Gariano, G.; Lesnyak, V.; Brescia, R.; Bertoni, G.; Dang, Z.; Gaspari, R.; De Trizio, L.; Manna, L. Role of the Crystal Structure in Cation Exchange Reactions Involving Colloidal Cu_2Se Nanocrystals. *J. Am. Chem. Soc.* **2017**, *139* (28), 9583–9590.

(35) Eikeland, E.; Blichfeld, A. B.; Borup, K. A.; Zhao, K.; Overgaard, J.; Shi, X.; Chen, L.; Iversen, B. B. Crystal Structure across the β to α Phase Transition in Thermoelectric $Cu_{2-x}Se$. *IUCrJ* **2017**, *4* (4), 476–485.

(36) Poulose, A. C.; Veeranarayanan, S.; Mohamed, M. S.; Aburto, R. R.; Mitcham, T.; Bouchard, R. R.; Ajayan, P. M.; Sakamoto, Y.; Maekawa, T.; Kumar, D. S. Multifunctional $Cu_{2-x}Te$ Nanocubes Mediated Combination Therapy for Multi-Drug Resistant MDA MB 453. *Sci Rep* **2016**, *6* (1), 35961.

(37) Li, D.; Wang, G.; Cheng, L.; Wang, C.; Mei, X. Engineering the Self-Assembly Induced Emission of Copper Nanoclusters as 3D Nanomaterials with Mesoporous Sphere Structures by the Crosslinking of Ce^{3+}. *ACS Omega* **2018**, *3* (11), 14755–14765.

(38) Katzbear, R. R.; Zhu, Y.; Mao, Z.; Schaak, R. E. Persistence and Evolution of Materials Features During Catalysis Using Topological and Trivial Polymorphs of $MoTe_2$. *ChemCatChem* **2022**, *14* (2).

Table of Contents Graphic

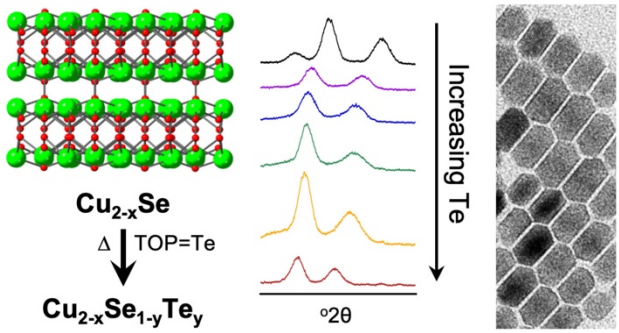

Synposis: Tellurium anion exchange of weissite $Cu_{2-x}Se$ nanoparticles with a trioctylphosphine-tellurium complex produces a morphologically and structurally conserved $Cu_{2-x}Se_{1-y}Te_y$ solid solution with tunable composition, rather than fully exchanged $Cu_{2-x}Te$. Over time, the solid solution composition transforms from Te-rich to Se-rich, which is coupled to changes in the surface chemistry and colloidal dispersity.